electronics

Article

Influence of Selected Factors on Thermal Parameters of the Components of Forced Cooling Systems of Electronic Devices

Krzysztof Posobkiewicz and Krzysztof Górecki *

Department of Marine Electronics, Gdynia Maritime University, Morska 81-87, 81-225 Gdynia, Poland; k.posobkiewicz@we.umg.edu.pl
* Correspondence: k.gorecki@we.umg.edu.pl; Tel.: +48-58-558-6448

Abstract: The paper presents some investigation results on the properties of forced cooling systems dedicated to electronic devices. Different structures of such systems, including Peltier modules, heat sinks, fans, and thermal interfaces, are considered. Compact thermal models of such systems are formulated. These models take into account a multipath heat transfer and make it possible to compute waveforms of the device's internal temperature at selected values of the power dissipated in the device. The analytical formulas describing the dependences of the thermal resistance of electronic devices co-operating with the considered cooling systems on the power dissipated in the cooled electronic device and the power feeding the Peltier module and the speed of airflow caused by a fan are proposed. The correctness of the proposed models is verified experimentally in a wide range of powers dissipated in electronic devices operating in different configurations of the used cooling system.

Keywords: thermal parameters; modelling; forced cooling systems; compact thermal model

check for updates

Citation: Posobkiewicz, K.; Górecki, K. Influence of Selected Factors on Thermal Parameters of the Components of Forced Cooling Systems of Electronic Devices. *Electronics* **2021**, *10*, 340. https://doi.org/10.3390/electronics10030340

Academic Editor: Vincenzo d'Alessandro

Received: 5 January 2021
Accepted: 26 January 2021
Published: 1 February 2021

1. Introduction

The problem that contemporary electronics still has to handle is effective cooling of electronic devices [1–5]. It is becoming even more important with an increase in the integration scale of semiconductor dies, dissipated power, and power density [6–9]. The cooling of semiconductor devices is critical due to self-heating phenomena causing an increment in semiconductor die temperature as a result of current flow across them [10–12]. As a result of self-heating, the internal temperature of semiconductor devices may reach values leading to a significant shortening of the device's lifetime and to its immediate catastrophic failure [13–15]. The solutions to reduce the value of the internal temperature of electronic devices are various cooling methods [5,16,17].

In general, cooling methods may be divided into two groups—passive (free cooling) and active (forced cooling) [16]. Free cooling methods use heat sinks, heat pipes [18–20], vapor chambers [18,20–26], liquid chambers [27], and various types of thermal interfaces —thermoconducting pastes, glues, pads, gels, and phase change materials [28,29]. Forced cooling methods mostly make use of fans, but also, liquid cooling systems [30–34] and thermoelectric (Peltier) modules [35,36] are used.

Forced and free cooling methods may be combined in many configurations of different complexities, costs, and efficiencies [30–34]. A cooling system may also operate in the free cooling mode until a certain level of temperature or power is reached, and in the forced cooling mode above that level. From the perspective of an engineer, when designing a cooling system, it is important to choose an optimal configuration of such a system. Computer modelling may help to solve the problem of selecting an optimal cooling system and to design it [37–40].

Thermal models allow the computation of the internal temperature of electronic devices at the known value of power dissipated in them. Both compact and detailed thermal models have been proposed in the literature [37–40]. Detailed thermal models allow the computation of time–spatial temperature distribution in the modelled device. In turn, compact models allow the computation of a waveform of one averaged internal temperature of the device.

Compact thermal models allow much faster computations, but they do not allow the computation of temperature distribution in the modelled device. In [41–44], a method of formulating compact models of semiconductor devices based on the result obtained by solving the heat transfer equation is proposed. In the cited papers, a multipath heat transfer in power modules or LED lamps is taken into account.

In [1], the problem of modelling the thermal properties of a system composed of an Insulated Gate Bipolar Transistor (IGBT) module, thermal interface, and heat sink is described. Compact thermal models in the form of both the Foster network and the Cauer RC network are used, and the revised method of measurements necessary to determine the thermal models' parameters is discussed. In turn, in [45] a similar problem is considered for a double-side cooled power module. In the cited paper, the results of the analyses performed with the Finite Element Method (FEM) are presented and discussed. It was shown that a multipath heat transfer should be taken into account.

The transfer of heat generated in electronic devices to the surroundings takes place by means of three mechanisms [10]: heat conduction, convection, and radiation. As indicated in [46,47], the efficiency of each mentioned way depends on the ambient temperature and internal temperature of the analyzed device.

Most compact thermal models proposed in the literature are linear and do not take into account the influence of temperature on the effectiveness of semiconductor devices' cooling. In the authors' previous papers [46,48], nonlinear thermal models of semiconductor devices operating in free cooling systems were proposed. In turn, in [47] a method of modelling a multipath heat transfer was proposed.

As it results from the literature review, the problem of modelling the thermal properties of forced cooling systems is not analyzed deeply. Particularly, the influence of the power dissipated in the cooled device and the parameters characterizing the efficiency of the components of the cooling systems are typically omitted. Therefore, investigations on the properties of such cooling systems should be performed.

In this paper, the results of such analyses illustrating the influence of selected factors on the parameters of a compact thermal model of selected cooling systems of electronic devices are presented. Investigations were carried out for various structures of cooling systems, including heat sinks, fans, thermal pads, and Peltier modules. It was proved that the nonlinear thermal models proposed in the paper reflect well the properties of the investigated cooling systems.

In Section 2, the used measurement method is described. Section 3 presents the investigated cooling systems. In Section 4, the elaborated thermal model is presented. Section 5 describes the method of parameter estimation. Section 6 presents the obtained results of the measurements and modelling of the considered cooling systems.

2. Measurement Method

In order to perform investigations, several cooling systems were selected. The general scheme of the experimental setup is shown in Figure 1.

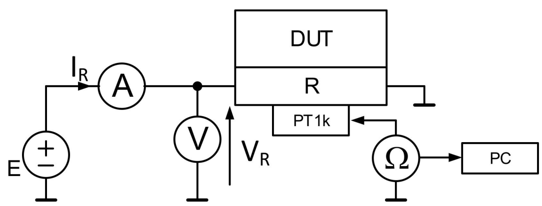

Figure 1. General scheme of the experimental setup.

As a heat source, a 3.6 Ω thick film resistor R with the ceramic substrate (Al_2O_3) GBR-666/12/2 by Telpod, Kraków, Poland [49] was used. This resistor has dimensions of 38 × 25 × 1 mm, and it is supplied from a voltage source E. Current I_R and voltage V_R on the resistor were measured using an ammeter and a voltmeter, respectively. The power dissipated in resistor R is equal to the product of I_R and V_R. The cooling systems selected for the investigations, presented in Figure 1 as DUT (Device under Test), are described in the next section.

Temperature T_R of resistor R was measured with a PT 1000 platinum temperature sensor (thermoresistor), Proffuse PT1000-550 (TME, Łódź, Poland) [50], glued to the surface of the resistive path in the middle of the resistor (see Figure 2). This thermoresistor is characterized by a tolerance of 0.3%, and the temperature coefficient of resistance α = 3850 ppm/K. The thermoconducting glue Amepox Microelectronic Thermopox 85CT (Amepox Microelectronic, Łódź, Poland) with a thermal conductivity in the range from 1.4 to 2.2 W/(m·K) and an electrical resistivity higher than 5 MΩ (with a thickness of over 0.1 mm) was used. The PT 1000 sensor resistance R_T was measured using an ohmmeter, UNI-T UT804 (Uni-Trend Technology (China) Co., Ltd., Dongguan, China). The temperature of this sensor was computed using the following formula:

$$T_R = T_0 + \frac{R_T - R_{T0}}{R_{T0} \cdot \alpha}, \tag{1}$$

where R_{T0} is the sensor resistance at reference temperature T_0 = 273.15 K. It was assumed that the PT 1000 sensor has a linear characteristic. A PC, the UNI-T UT804 multimeter, and the dedicated software were used to record a transient thermal response $T_R(t)$ of the considered resistor co-operating with the investigated cooling systems.

Figure 2. General view of the investigated resistor with a mounted temperature sensor.

In order to measure the thermal parameters of this device operating in different cooling systems, the following steps should be performed:

a) Measurement of resistance R_{T1} of the thermoresistor at the steady state when the investigated resistor is not fed (I_R = 0);
b) Computation of the value of temperature T_{R1} corresponding to resistance R_{T1} using Equation (1);
c) Feeding this resistor with heating power until the steady state is obtained; in this step, the values of voltage V_R and current I_R are measured at the steady state, whereas waveform $R_T(t)$ is recorded using a multimeter and a PC;
d) Computation of the waveform of the transient thermal impedance of the investigated resistor using the following formula:

$$Z_{th}(t) = \frac{R_T(t) - R_T(t=0)}{R_{T0} \cdot \alpha \cdot V_R \cdot I_R} \tag{2}$$

The value of transient thermal impedance $Z_{th}(t)$ at $t \to \infty$ is equal to thermal resistance R_{th}.

3. Investigated Cooling Systems

Investigations were performed for the considered power resistor co-operating with five different cooling systems. One of them belongs to free cooling systems, whereas the other four to forced cooling systems. These cooling systems are characterized below.

The simplest free cooling system, denoted further as system A, contains only the investigated resistor. It is mounted as it is shown in Figure 2. In turn, the cooling system denoted as system B contains the resistor, an active heat sink, and a self-adhesive thermo-conducting pad used as a thermal interface. System C contains the tested resistor, a heat sink, and a silicon paste applied as a thermal interface. System D contains the investigated resistor, an active heat sink, and a self-adhesive thermoconducting pad operating as a thermal interface. System E contains the tested resistor, the Peltier module, an active heat sink, and two self-adhesive thermoconducting pads as thermal interfaces.

In cooling systems D and E, the Peltier module (Ferrotec Nord, Moscow, Russia) TM–71-1.4-8.5MS was used. According to the producer's data [51], the dimensions of this module are 30 mm$\times$ 30 mm $\times$ 3.4 mm, whereas the maximum feeding current I_{max} = 8.5 A, the maximum feeding voltage V_{max} = 8.2 V, the maximum dissipated power P_{max} = 41.8 W, and the maximum difference in temperature between the two module sides ΔT_{max} = 71 °C. In systems B, D, and E, a double-side self-adhesive thermoconducting pad, THERMOPAD-6X1X30 (TME, Łódź, Poland) [52], with thermal conductivity λ = 6 W/(m·K) was used. The pad is 1 mm thick (d = 1 mm), and its nominal thermal resistance can be computed using the following formula:

$$R_{thtp} = \frac{d}{\lambda \cdot S} = \frac{0.001m}{6W/m \cdot K \cdot 0.0009m^2} = 0.1852K/W \quad (3)$$

where S is the area of this pad.

The view of cooling system D is shown in Figure 3.

Figure 3. View of cooling system D.

The Peltier module is fed from the current source I_P. The module's current I_P and voltage V_P are measured with an ammeter and a voltmeter. The power dissipated in this module is equal to the product of current I_P and voltage V_P.

In cooling systems B, C, and E, the PC microprocessor active heat sink Arctic Freezer 34 eSports Duo 2 $\times$ 120 mm [53] containing a heat sink and a fan were used (see Figure 4). Systems B and C differ from each other in the type of thermal interface used between the resistor and the active heat sink, which in system B is the pad described above and in system C the thermoconducting paste Electrolube EHTC10S of thermal conductivity $\lambda = 0.9$ W/(m·K). In order to hold the investigated cooling system in a fixed position, systems B, D, and E were held in a vice using teflon separators. In order to fix the heat source in its place in system E, a back frame coming as a part of the Arctic cooling set was used. To achieve the appropriate value of the press force, two thermally insulating separators were used.

Figure 4. General view of cooling systems with the Arctic Freezer 34 eSports Duo.

The Arctic cooling set is constructed with the use of a heat sink made of a stack of aluminum fins attached to four heat pipes and two fans of 120 mm diameter each. The base of the set is constructed with an aluminum block with heat pipes going across it [50]. In order to achieve the best possible heat conduction from the heat source to the heat sink, the heat pipes are shaped and machined in the so-called direct contact technique.

The two fans of the Arctic cooling set are supplied from the external voltage source. The voltage on the fans is controlled with a voltmeter. In this configuration, the speed of the air is measured.

The view of cooling system C is shown in Figure 5, whereas the view of system E in Figure 6.

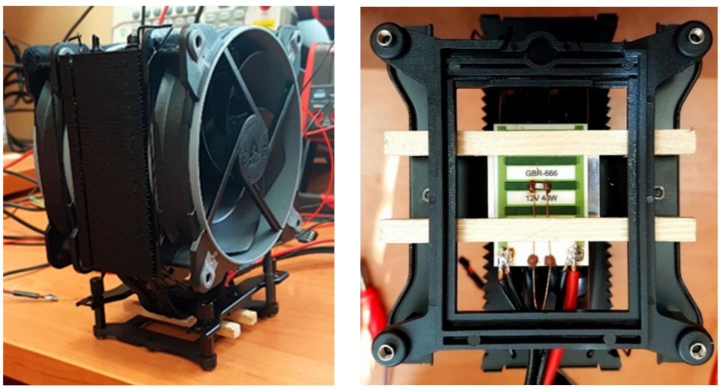

(**a**) (**b**)

Figure 5. View of cooling configuration C—general (**a**) and from the heat source side (**b**).

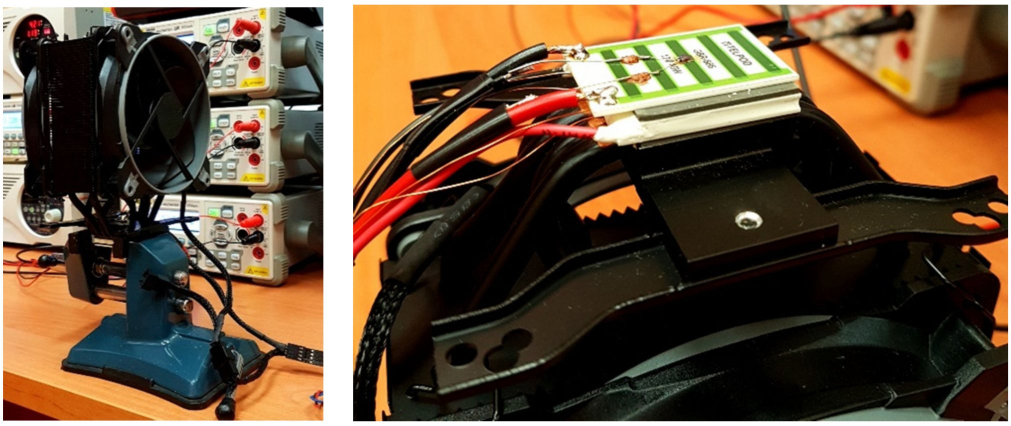

(**a**) (**b**)

Figure 6. General view of cooling configuration E (**a**) and view of the heat source (**b**).

4. Thermal Model

In order to analyze the thermal properties of the cooling systems under investigation, a nonlinear thermal model of the investigated cooling system was proposed. This model allows the computation of internal temperature T_j of the electronic device at the known power dissipated in it, taking into account the influence of ambient temperature power loses in the modelled device and in the parts of the cooling system (e.g., Peltier module) and the speed of the air around the heat sink on the efficiency of heat removal.

The model has the form of a subcircuit for Simulation Program with Integrated Circuits Emphasis (SPICE). At its formulation, the electrical–thermal analogy presented (e.g., in [39,54,55]) was applied. In this analogy, voltage represents temperature; current, power; resistance, thermal resistance; and capacitance, thermal capacitance. The formulated model is based on the idea proposed in [46,56]. According to this idea, the nonlinear Foster network is used to model the dependence of the transient thermal impedance of this device on the dissipated power. Due to the fact that an influence of the considered parameters on thermal resistances was observed and such an influence was not observed for thermal capacitances, in the model proposed in this paper, linear thermal capacitances and nonlinear thermal resistances were used.

A network representation of the proposed nonlinear thermal model of the electronic device is shown in Figure 7.

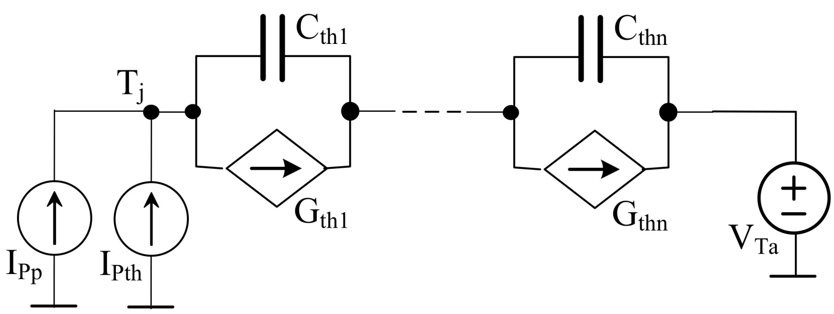

Figure 7. Network representation of a nonlinear thermal model of the electronic device.

In this model, current source I_{Pth} represents the power dissipated in the modelled device; current source I_{Pp}, the power dissipated in the Peltier module; voltage source V_{Ta}, ambient temperature; controlled current sources $G_{th1}, \ldots, G_{thn}$, the components of thermal resistance of this device; and capacitors $C_{th1}, \ldots, C_{thn}$, thermal capacitances of the components on the heat flow path.

The ability of the modelled device to dissipate heat generated inside this device with all the mechanisms of heat transfer is characterized by transient thermal impedance $Z_{th}(t)$, typically given in a form of the formula [39,54,55]

$$Z_{th}(t) = R_{th} \cdot \left[1 - \sum_{i=1}^{N} a_i \cdot \exp\left(-\frac{t}{\tau_{thi}}\right)\right], \quad (4)$$

where R_{th} is thermal resistance, a_i are coefficients corresponding to thermal time constants τ_{thi}, and N is the number of thermal time constants.

Thermal capacitances in this model depend on the kind of material and mass of the components occurring in the heat flow path of the cooling system [10]. The parameters of the components of the cooling system mentioned here do not change much with temperature changes. Therefore, capacitors modelling thermal capacitances are linear in the proposed model. In turn, thermal resistances R_{th} in the model depend on many factors (e.g., the construction of the cooling system applied and power losses in the cooled device). These thermal resistances are characterized in the latter part of this section.

Changes in the values of thermal resistance are modelled by controlled current sources $G_{th1}, \ldots, G_{thn}$. The current of such a source is given by the following formula

$$G_{thi} = V_{Gi}/(a_i \cdot R_{th}), \quad (5)$$

where V_{Gi} denotes the voltage on current source G_{thi}.

Thermal capacitances are given by the following formula:

$$C_{thi} = \tau_{thi}/(a_i \cdot R_{th}). \quad (6)$$

In the presented model, the dependence of R_{th} on dissipated power p_{th} is described with the use of the empirical formula of the following form:

$$R_{th} = \left(R_{th0} + R_{th1} \cdot \exp\left(-\frac{p_{th}}{b}\right) + \frac{p_{th}}{c}\right) \cdot a_x \cdot b_x \quad (7)$$

where R_{th0} denotes the minimum value of thermal resistance, whereas R_{th1}, b, and c are model parameters. The values of parameters R_{th0}, R_{th1}, b, and c depend on the configuration of the investigated cooling system.

When the Peltier module is a part of the cooling system, parameter a_x depends on the power feeding the module according to the formula

$$a_x = 1 + \alpha_{thP} \cdot \exp\left(-\frac{p_P}{b_P}\right), \quad (8)$$

where p_P means the power feeding the Peltier module and α_{thP} and b_P are parameters of the thermal model of the module.

In turn, when a fan is used in the cooling system, b_x depends on the speed of the airflow generated by the fan according to the formula

$$b_x = 1 + \beta_{thv} \cdot \exp\left(-\frac{v}{b_v}\right), \quad (9)$$

where β_{thv} and b_v are parameters of the thermal model characterizing the influence of airflow speed v on thermal resistance.

5. Model Parameters Estimation

In order to practically use the proposed model, the values of the parameters occurring in this model should be estimated. The estimation procedure consists of three steps. First, the waveforms of the transient thermal impedance of the investigated device are measured with the use of the method described in Section 2. These measurements should be performed for the used cooling system at different values of the power dissipated in this device.

In the second step, parameters R_{th}, N, a_i, and τ_{thi}, occurring in Equation (4), are estimated with the use of the ESTYM algorithm described in the paper [39]. The values of parameters R_{th}, a_i, and τ_{thi} obtained at the highest value of the dissipated power are used to compute the values of thermal capacitances C_{thi} using Equation (6). Additionally, the values of parameters a_i are used to describe the output current of sources G_{thi}.

In the third step, the measured dependences $R_{th}(p_{th})$ are approximated using the formula (7) for the used cooling systems. For the maximum value of power p_{th}, $R_{th}(p_p)$, and $R_{th}(v)$, the parameters occurring in Equations (8) and (9) are estimated using the measured dependences. For cooling systems without the Peltier module, parameter $\alpha_{thP} = 0$, whereas for such systems without fans, parameter $\beta_{thv} = 0$.

Figures 8–15 present the measured (points) and modelled (lines) dependences $R_{th}(p_{th})$ for all the considered cooling systems. The modelled curves are obtained using the estimated values of the model parameters.

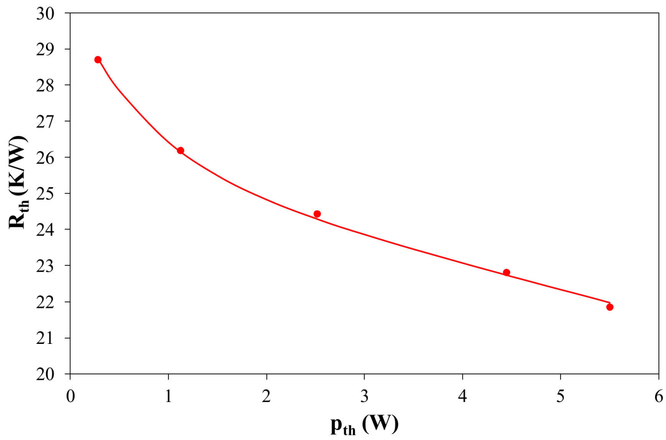

Figure 8. Measured and modelled dependences of the thermal resistance of the resistor operating without any cooling system on the power dissipated in this resistor (system A).

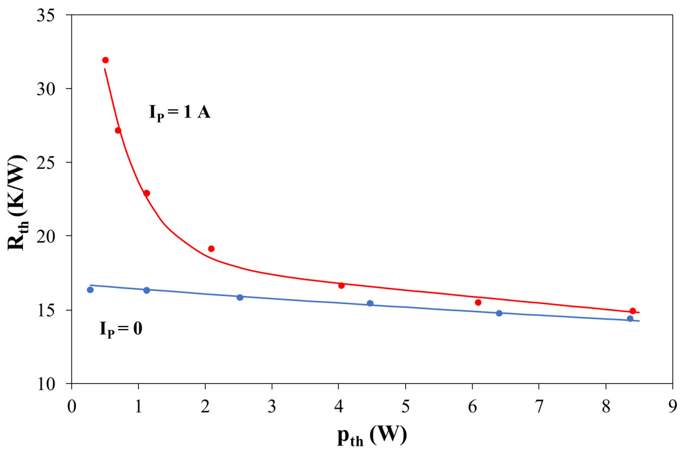

Figure 9. Measured and modelled dependences of the thermal resistance of the resistor co-operating with the Peltier module on the power dissipated in this resistor at selected values of current I_P (system D).

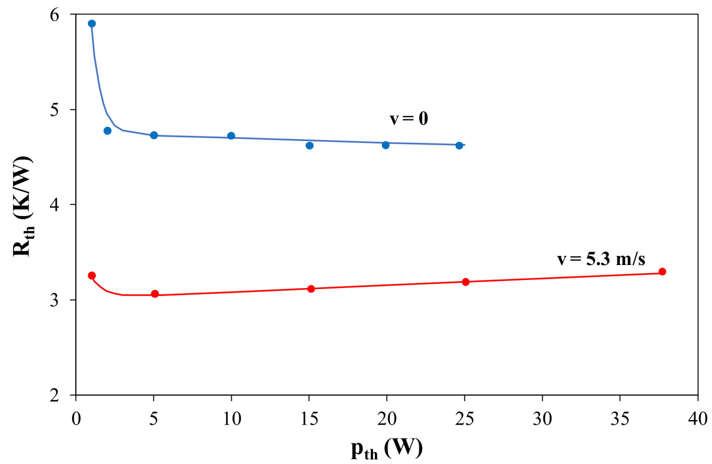

Figure 10. Measured and modelled dependences of the thermal resistance of the resistor situated on the heat sink with a fan on the power dissipated in the resistor at selected values of the airflow speed (system B).

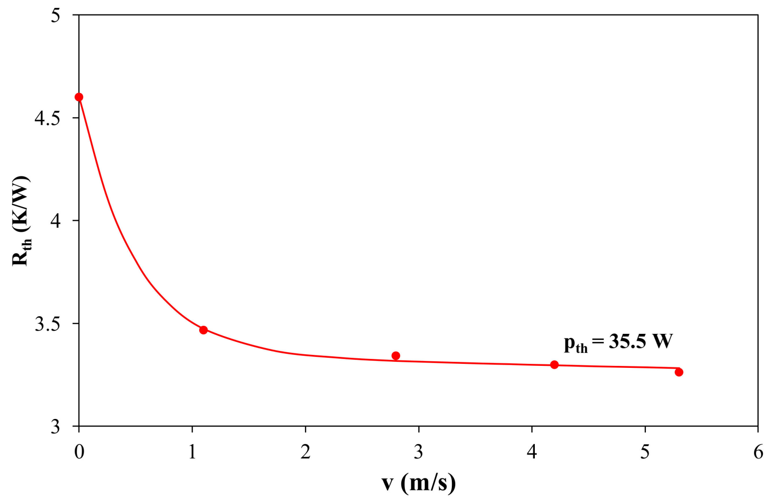

Figure 11. Measured and modelled dependences of the thermal resistance of the resistor placed on the heat sink with a fan on the airflow speed at power p_{th} = 35.5 W (system B).

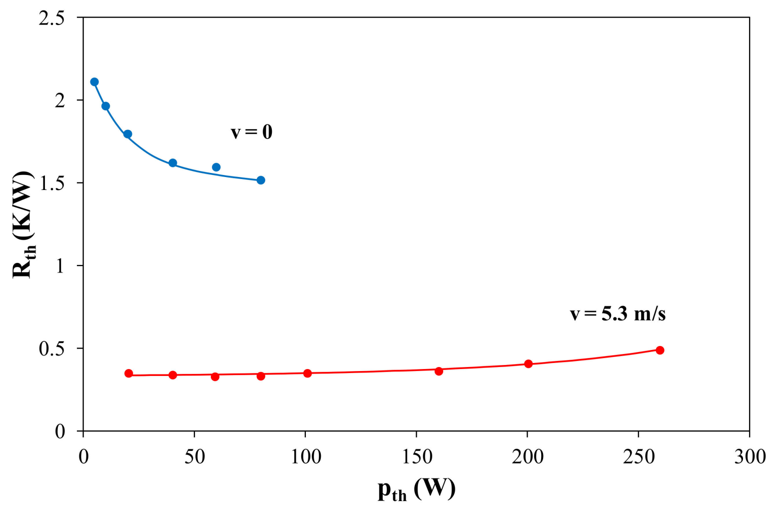

Figure 12. Measured and modelled dependences of the thermal resistance of the resistor mounted on the heat sink with a silicon paste on the dissipated power at selected values of the airflow speed (system C).

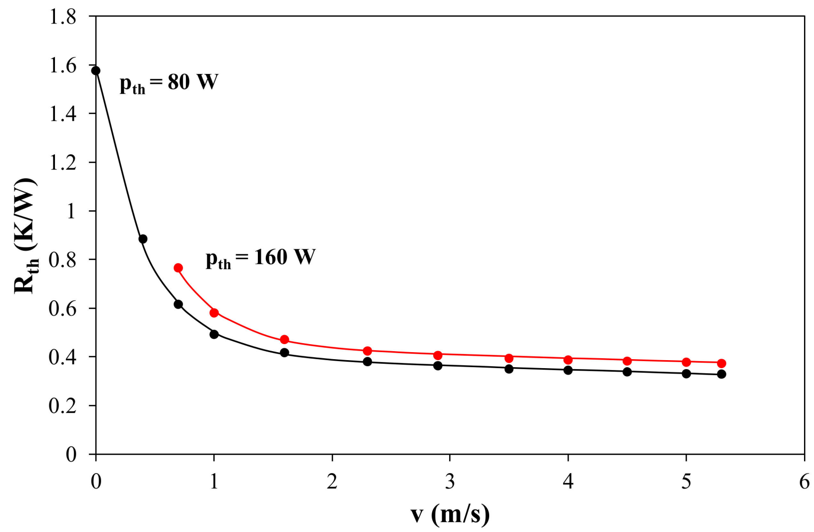

Figure 13. Measured and modelled dependences of the thermal resistance of the resistor mounted on the heat sink with a silicon paste on the airflow speed at selected values of the dissipated power (system C).

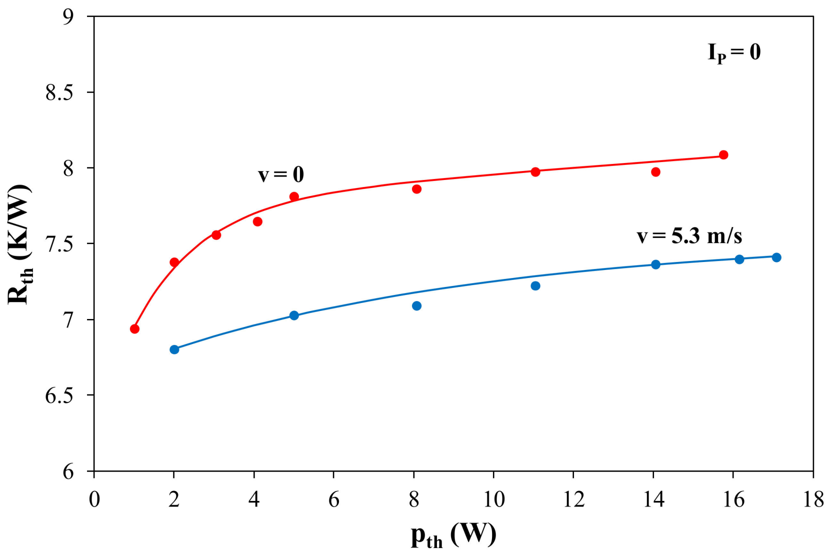

Figure 14. Measured and modelled dependences of the thermal resistance of the resistor mounted on the heat sink with two thermal pads and the Peltier module on the dissipated power at selected values of the airflow speed (system E).

Figure 8 illustrates the dependence of the thermal resistance of a power resistor placed horizontally and operating without any additional cooling (system A) on power p_{th} dissipated in this resistor.

As may be noticed, dependence is a monotonically decreasing function. In the considered range of the dissipated power, thermal resistance decreases by about 25% (from 29 K/W to 22 K/W). The observed dependence is a result of a rise in the efficiency of natural convection on the surface of the investigated resistor with an increment of its temperature.

Figure 9 presents the measured and modelled dependences of the thermal resistance of the resistor attached to the cold side of the Peltier module with the use of a thermal pad (system D). This figure shows also an influence of the power dissipated in the Peltier module on the thermal resistance of the investigated resistor. The results obtained for the Peltier module with no supply (I_P = 0) are marked with blue color, whereas the results for the module's current I_P = 1 A are marked with red color.

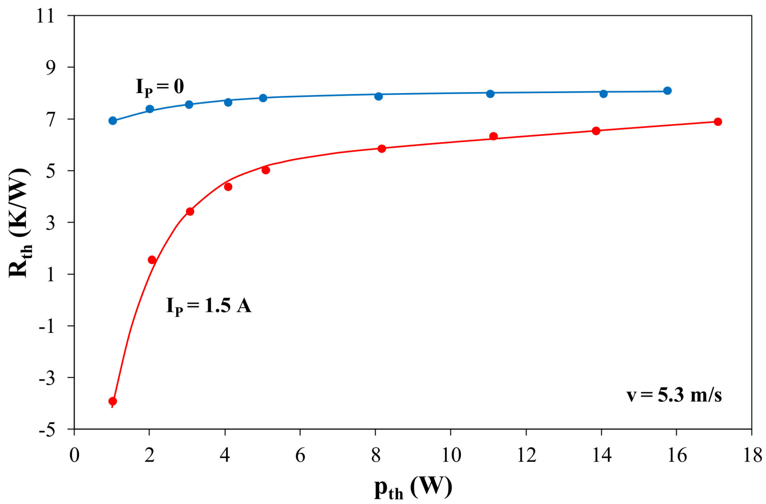

Figure 15. Measured and modelled dependences of the thermal resistance of the resistor operating in system E on the dissipated power at selected values of the current feeding the Peltier module (system E).

For both values of the module's current, thermal resistance is a decreasing function of the dissipated power. In particular, at I_P = 1 A an influence of the value of the dissipated power on thermal resistance is clearly visible. It results from the fact that the hot side of the Peltier module was cooled in a way of natural convection and no heat sink was attached to it. Additionally, in the considered cooling system, power was dissipated both in the resistor and in the Peltier module, causing a bigger growth of the resistor temperature than in the case when this module was not supplied. At low values of power p, the power dissipated in the Peltier module is a dominant component of the whole power dissipated in the investigated cooling system. It is worth noting that attaching the Peltier module using a thermal pad allowed the reduction of the thermal resistance value even by 50% compared with a resistor with no cooling system attached. It is probably a result of a growth in the heat exchange area.

The results of investigations on the next cooling system (system B) containing the considered resistor, the thermal interface, and a heat sink with a fan are shown in Figures 10 and 11. Figure 10 shows the dependences of the thermal resistance of the resistor operating in the analyzed system on the power generated in the resistor at two values of the airflow speed equal to 0 (blue) and 5.3 m/s (red).

The presented dependence $R_{th}(p_{th})$ is a decreasing function in the whole range of power p_{th} when the cooling system operates in the natural convection (v = 0) conditions, whereas at operation in the forced convection conditions (v = 5.3 m/s), an increasing function $R_{th}(p_{th})$ is obtained for power p_{th} > 3 W. Such a character of $R_{th}(p_{th})$ changes indicates that in the natural convection conditions, heat convection has a dominant influence on thermal resistance, but in the forced cooling conditions, it is heat conduction. It is worth noting that applying forced cooling allows the lowering of the thermal resistance of the resistor even by 35%.

Figure 11 presents the dependence of the thermal resistance of the resistor incorporated into the investigated cooling system on the airflow speed at power p_{th} = 35.5 W dissipated in the resistor.

It can be noticed that dependence $R_{th}(v)$ is a decreasing function in the whole analyzed range of the airflow speed changes. It is important to point out that the biggest change in thermal resistance is observed at low values of airflow speed v. For example, a change of the airflow speed in the range from 0 to 1 m/s causes a decrease of R_{th} by 25%, whereas a change from 1 to 5 m/s causes a change of R_{th} only by 6%.

Figures 12 and 13 illustrate the thermal properties of the investigated resistor cooled by an active heat sink. As the thermal interface between the resistor and the heat sink, the silicon paste is applied (system C). In Figure 12, the dependence of the thermal resistance of the resistor operating in this cooling system on the power generated in it at two values of airflow speed v equal to 0 and 5.3 m/s is shown.

As can be noticed, dependence $R_{th}(p_{th})$ is an increasing function at airflow speed v = 5.3 m/s, and it is a decreasing function at v = 0. The considered increment in airflow speed causes over a triple decrease in the value of the thermal resistance. At v = 0, an increase in the dissipated power from 5 to 80 W causes a decrease in the value of R_{th} by 25% due to an increase in the efficiency of heat convection as a result of a higher temperature of the surface of the resistor. In turn, at v = 5.3 m/s, an increase in the dissipated power from 15 to 260 W causes an increment in the R_{th} value exceeding by even 40%. This change is a result of a decrease in the thermal conductivity of the heat sink due to a higher temperature of the resistor.

The results presented in Figure 12 prove that applying the silicon paste instead of a thermal pad allows the reduction of the thermal resistance value even by about 2.5 K/W, which means that it is possible to raise the power dissipated in the resistor even three times.

In Figure 13, the dependence of the thermal resistance of the resistor on the airflow speed at two values of power equal to 80 and 160 W is shown.

As can be seen, an increase in the airflow speed causes a decrease in the thermal resistance of the resistor. In the considered range of changes of the airflow speed, R_{th} decreases from 1.6 K/W to 0.3 K/W. The biggest change is observed in the range of speed from 0 to 1.5 m/s.

Figures 14 and 15 show the measurements and modelling results of the cooling system containing the resistor selected for the experiment, the Peltier module, an active heat sink, and two thermal pads (system E). In Figure 14, the dependences of the thermal resistance of the resistor on the power dissipated in the resistor without feeding the Peltier module and two values of the airflow speed equal to v = 0 and v = 5.3 m/s are presented.

As can be seen, the obtained values of thermal resistance are highest of all the considered systems of forced cooling. This is a result of the use of additional layers on the heat flow path—two thermal interfaces and the Peltier module. Dependence $R_{th}(p_{th})$ is an increasing function in the whole range of changes of the dissipated power. An increment in the airflow speed causes an increase in thermal resistance even by 10%.

Figure 15 illustrates the influence of the current supplying the Peltier module on dependence $R_{th}(p_{th})$ at two selected values of current I_P feeding this module.

For both I_P values, increasing dependences $R_{th}(p_{th})$ were obtained. In the figure, the negative R_{th} value for power p_{th} < 2 W draws attention. It is a result of applying the Peltier module, whose cold side is in contact with the resistor via a thermal pad. In this range, the power dissipated in the resistor is so small that an increase in its temperature caused by self-heating is smaller than a temperature drop caused by the Peltier module.

For each of the cooling systems operating at different conditions, the values of thermal capacitances C_{thi} were estimated. The number of these capacitances depends on the structure of the considered system. For example, in the model of system B-2, thermal capacitances occur, and in the model of system E-3, thermal capacitances occur. The values of particular thermal capacitances describing the properties of the same cooling system change not more than by a small percentage with changes of the power dissipated in the cooled device.

6. Results

In order to validate the proposed thermal model, some measurements and computations of temperature of a power resistor co-operating with various cooling systems were performed. The results of the investigations are presented in the figures shown in the latter part of this section. In all these figures, points denote the results of the measurements, whereas lines, the results of the computations.

Figure 16 illustrates the waveforms of temperature $T_R(t)$ of the resistor operating in system A and excited with a power step of various values of p_H equal to 2.5 W, 4.4 W, and 5.5 W.

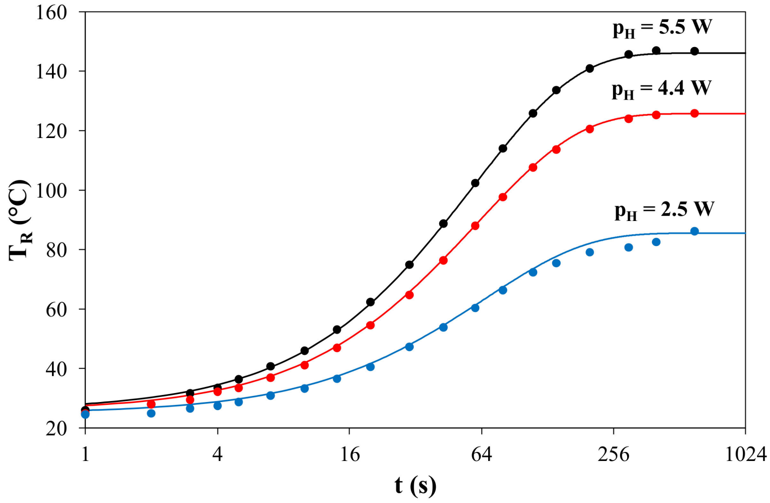

Figure 16. Measured and computed waveforms of the temperature of the resistor operating in cooling system A at selected values of the power dissipated in the resistor (system A).

It can be easily noticed that the computed waveforms $T_R(t)$ are modelled with a very good accuracy for all the power values. The time necessary to achieve the steady state does not exceed 500 s, and the resistor temperature in the steady state at the highest value of power reaches almost 150 °C.

In Figure 17, the computed and measured waveforms of the considered resistor temperature for three different ways of power generation in the investigated cooling system D are presented. Blue color corresponds to the case when power p_H = 8.4 W is generated only in the resistor, black color when power P_p = 1.7 W is generated only in the Peltier module, and red color when power is generated both in the resistor (p_H = 6.1 W) and in the Peltier module (P_p = 2 W).

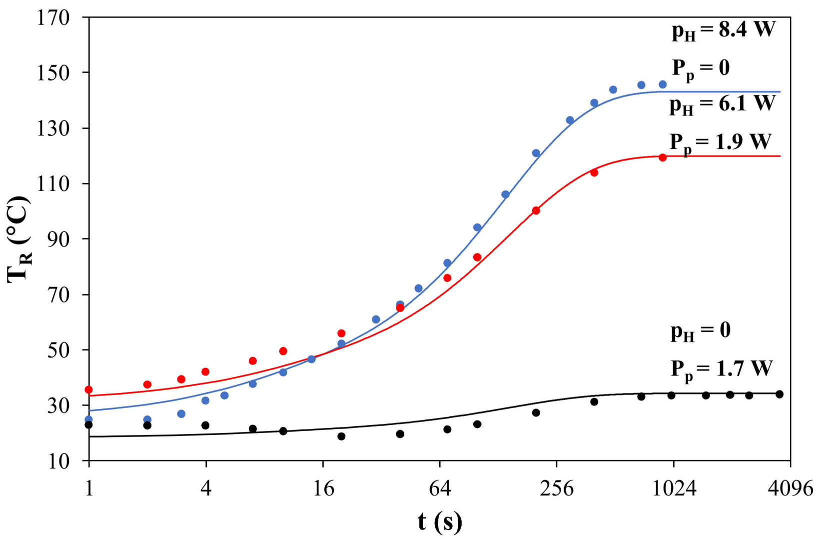

Figure 17. Measured and computed heating curves of the internal temperature of the resistor operating with the Peltier module (system D).

Analyzing the obtained waveforms $T_R(t)$, it can be noticed that when power is generated only in the Peltier module, in a short time (between 6 and 60 s) after switching the cooling system on, the temperature of the resistor decreases below the ambient temperature. Later, this temperature increases as a result of heat generation in the Peltier module and heating up of the resistor by the module. When power is generated only in the resistor, the obtained values of temperature T_R are highest. When the power of a similar overall value is generated in the resistor and in the Peltier module, the resistor temperature is lower than when the power is generated only in the resistor.

It is worth noting that applying the Peltier module in the cooling system allowed the improvement of the efficiency of heat dissipation, but simultaneously, the power generated in the cooling system increased, which may cause an additional rise in temperature in the cooled device. In the analyzed cooling system, the steady state is reached after about 1000 s.

In Figure 18, the waveforms of the internal temperature of the power resistor cooled by a heat sink equipped with a fan (system B) is shown. Waveforms $T_R(t)$ correspond to two values of the power generated in the cooled resistor (25 W and 37.7 W) and two values of the airflow speed v (0 and 5.3 m/s).

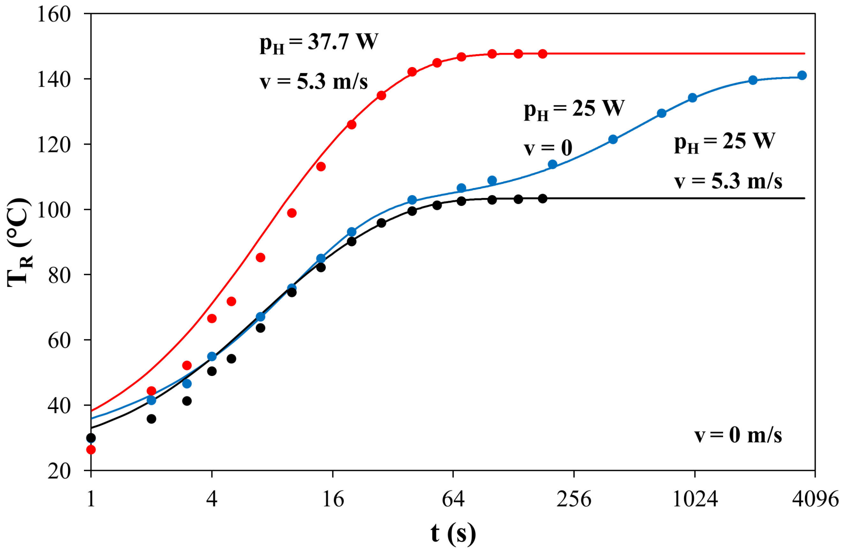

Figure 18. Measured and computed heating curves of the internal temperature of the resistor situated on the heat sink with a fan (system B).

As can be seen, at a higher speed of the considered speeds of the airflow, temperature T_R stabilizes after 1 min after the measurements start. In contrast, in the natural convection conditions (v = 0), the time of temperature $T_R(t)$ stabilization exceeds 1 h. At power p_{th} = 25 W generated in the tested resistor, due to the application of forced cooling, temperature T_R in the steady state is about 35 °C lower than that for power p_H = 37.7 W.

Figure 19 illustrates the waveforms of the internal temperature of the resistor selected for the experiment heated with a power of 81.7 W at two values of the airflow speed equal to 0 (blue color) and 5.3 m/s (red color).

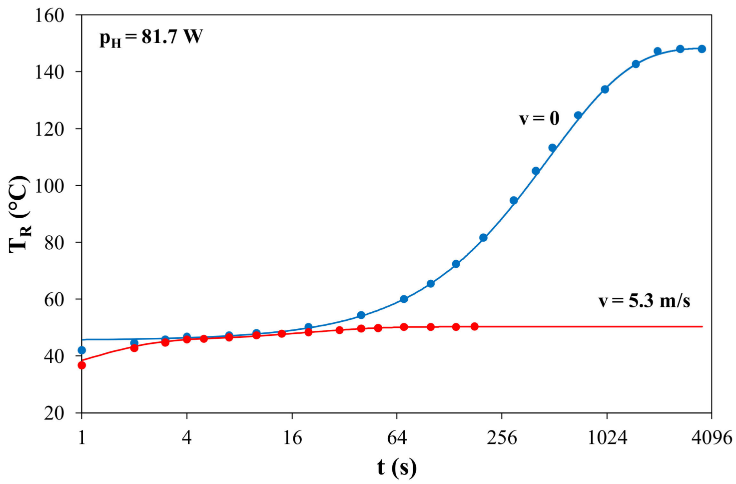

Figure 19. Measured and computed heating curves of the internal temperature of the resistor mounted on the heat sink with a silicon paste (system C) at selected values of the airflow speed.

Comparing the results obtained for both values of v, it can be noticed that the airflow speed significantly influences both the temperature of the resistor at the steady state and the time of $T_R(t)$ stabilization. At a higher value of the two considered values of the airflow speed, this time is equal to merely 30 s and 1 h at $v = 0$. The values of T_R temperature at the steady state differ from each other even by about 100 °C.

In Figure 20, the measured and computed heating curves of the internal temperature of the resistor selected for the experiment with cooling system E composed of an active heat sink, the Peltier module, and two thermal pads at two values of the Peltier module's current $I_P = 0$ and $I_P = 1.5$ A are shown.

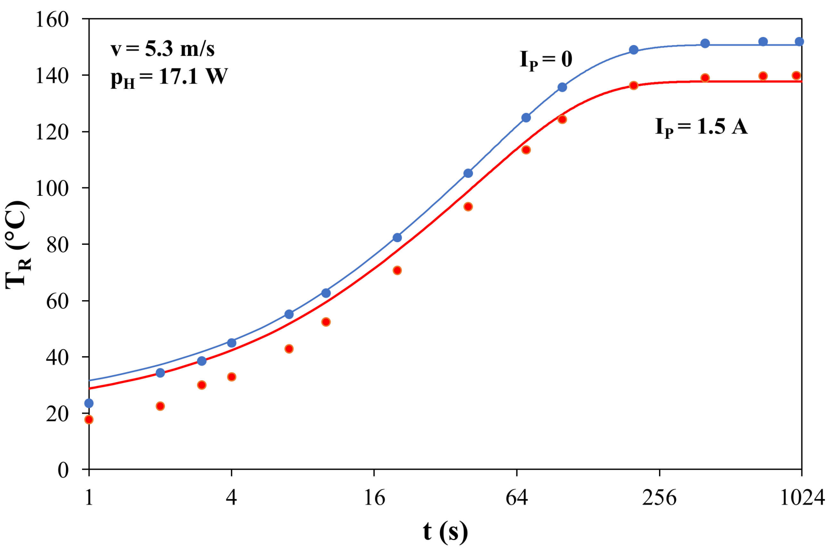

Figure 20. Measured and computed heating curves of the internal temperature of the resistor with cooling system E at two values of the Peltier module's current (system E).

As can be seen, the temperature stabilization time is about 400 s in both cases. Feeding the Peltier module with current $I_P = 1.5$ A causes a 12 °C drop in the resistor temperature.

Analyzing the results of the investigations presented above, one can conclude that the construction of the cooling system significantly influences the ability of an electronic device to dissipate the heat generated in this device.

In Figure 21, the measured and computed dependencies of the thermal resistance of the considered resistor on the power dissipated in this device are presented. In this figure, the results related to each cooling system are marked in the following way: system A, the investigated resistor with no additional cooling devices; system D, constructed with a thermal pad and the Peltier module; system E, constructed with two thermal pads, the Peltier module, and an active heat sink; system B, constructed with a thermal pad and an active heat sink; system C, constructed with a thermoconducting paste and an active heat sink. The curves in the figure are also marked with the values of the parameters characterizing the cooling process.

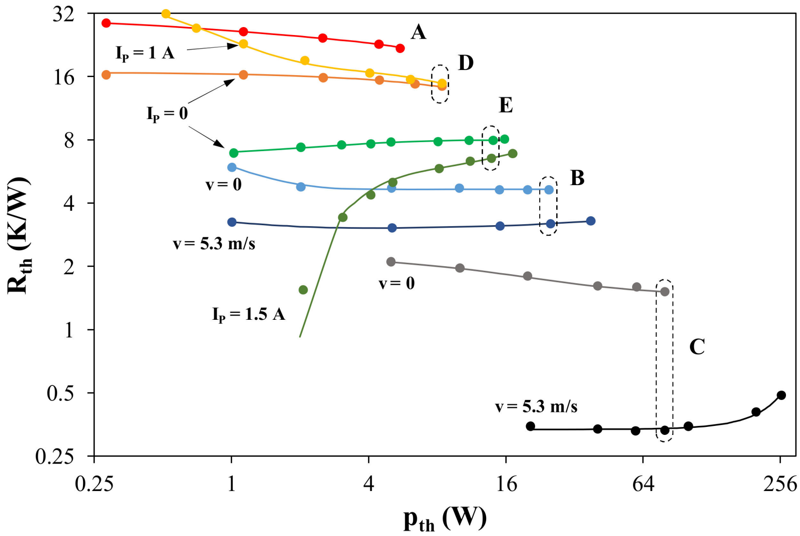

Figure 21. Measured and computed dependences of the thermal resistance of the resistor on the dissipated power in all the investigated cooling systems.

Analyzing the results of the investigations presented in this paper, one can see that the proper selection of a cooling system allows the reduction of the values of the thermal resistance of the resistor selected for the tests almost 100 times. It can also be noticed that the maximum power that can be dissipated in the resistor without exceeding its maximum allowable temperature goes up from 5 W to over 250 W.

Obviously, cooling was least efficient in system A (i.e., in the case of the resistor without any additional components improving the heat dissipation in it). Adding the Peltier module and a thermal pad to this system allows the improvement of the efficiency of cooling due to a growth of the heat convection area. A further drop of thermal resistance is achieved after adding an active heat sink on top of the cooling system. As it turned out, the removal of the Peltier module and the thermal pad from the cooling system improved the investigated device's cooling efficiency. It is worth noting that the thermal pad applied is responsible for an important part of the overall thermal resistance. Replacing this pad with the silicon paste allows the reduction of thermal resistance even by 2 K/W.

It is also easy to observe that in the operation of the cooling system in the free convection conditions when neither the Peltier module nor the fan is fed, dependence $R_{th}(p_{th})$ is a decreasing function. It allows the conclusion that the dominant component of thermal resistance is connected to heat convection. According to the equation given (e.g., in [10,57,58]), the efficiency of heat removal with heat convection is proportional to the difference between the temperatures of the cooled surface and the cooling fluid. Of course, the temperature of the cooled surface goes up with an increase in the dissipated power at the fixed cooling conditions. In turn, in the forced cooling systems used, where the Peltier modules or a fan is supplied, dependence $R_{th}(p_{th})$ is an increasing function. This character of the considered dependence indicates that the dominant component of thermal resistance is connected to heat conduction, whose efficiency for the materials used to construct heat sinks decreases with temperature rise. According to the considerations given (e.g., in [10,57,58]), the efficiency of heat removal with heat conduction is a decreasing function of the device temperature. This temperature goes up with an increase in the dissipated power.

A good match of the results of the measurements and computations is obtained for all the considered cooling systems, which proves that the proposed model equations are correct.

In order to compare the effectiveness of the investigated cooling systems, the values of an excess of the temperature of the considered resistor over the ambient temperature at the fixed value of the dissipated power p_{th} = 5.5 W are presented in Figure 22.

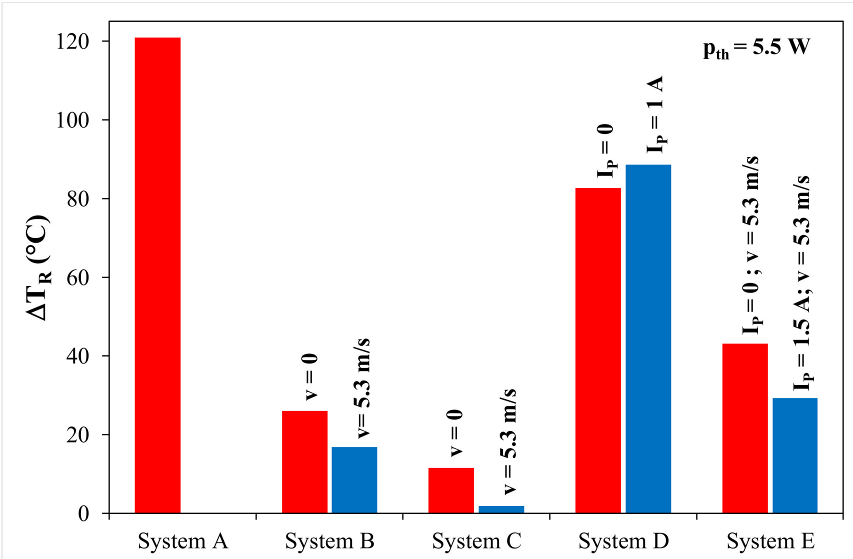

Figure 22. Values of an excess of the temperature of the considered resistor over the ambient temperature for the fixed value of the dissipated power for all the investigated cooling systems.

It is easy to observe that the highest value of the resistor temperature is obtained for system A, without any components improving the cooling. In this case, ΔT_R = 120 °C. The most efficient is the cooling of system C, in which the value of ΔT_R does not exceed 2 °C. It is shown that the considered forced cooling systems can make it possible to reduce temperature excess ΔT_R by even 60 times in the device.

From the point of view of the designer of cooling systems, not only is the efficiency of these systems important, but also the costs and dimensions of the used components should be taken into account. In the considered cooling systems, the cost of a thermal pad is equal to 1.5 USD; the Peltier module, 23 USD; and the active heat sink, 51 USD. The volumes of these components are 0.9 cm^3, 3.06 cm^3, and 2005.2 cm^3, respectively. It is shown that in order to obtain the best cooling efficiency, the active heat sink is needed, which is characterized by the highest cost and the greatest volume.

7. Conclusions

In this paper, a way of modelling the thermal properties of an electronic device operating in the free convection and forced convection conditions is presented. A form of a nonlinear compact thermal model and equations describing the influence of selected factors on the thermal resistance of the electronic device are proposed. Validation of the proposed model was performed experimentally in five cooling systems. For each system, a good match of the results of the measurements and computations was achieved. The differences between these results typically do not exceed 5%.

The results presented in the paper prove that the selection of cooling system components influences the ability to dissipate heat generated in the cooled device, which is characterized by thermal parameters. It was shown that additional components of the cooling system do not always improve the efficiency of heat dissipation. This concerns in particular the use of the Peltier module and thermal pads. Thermal pads provide electrical insulation between cooling system components, but they also cause a significant rise in thermal resistance, even equal to about 2 K/W.

The performed measurements and computations show that applying a cooling system based on natural convection provides efficient dissipation of the heat generated in the electronic device, but systems based on forced convection provide further reduction of thermal resistance. The value of this parameter can be reduced by even 100 times, whereas the dissipated power can increase by even 50 times due to the modification of the cooling system.

It was shown that with the power generated in the cooled device, the current supplying the Peltier module and the airflow speed significantly influence the thermal resistance of the cooled device. This influence was modelled with exponential functions, which allowed us to obtain a very good match of the results of the measurements and computations.

It is worth noting that in forced cooling systems, the dependence of thermal resistance on the dissipated power is a monotonically increasing function, and in free cooling systems, it is a decreasing function. This results from the dominant influence of convection on heat dissipation in such systems and thermal conduction in forced cooling systems.

For the investigated cooling systems, the time of temperature stabilization in an electronic device is much longer in free cooling systems than in forced cooling systems. This time varies by even 100 times when comparing both the considered groups of cooling systems.

The results of the investigations presented in the paper may be used by designers of cooling systems of electronic devices. These results may make easier the selection of the cooling system components of an electronic device appropriate for the dedicated application.

The computations and measurements were performed for the resistor with dimensions of 38 mm $\times$ 25 mm $\times$ 1 mm, but the influence of the considered factors on the thermal parameters of the electronic devices would be quantitatively the same for such devices with different dimensions. Particularly, the influence of the dissipated power on the thermal resistance of power semiconductor devices can be described with an exponential function [47].

In further considerations, the usefulness of the thermal model proposed in this paper for power semiconductor devices will be analyzed. Additionally, the influence of the dimensions of the components of a forced cooling system on the thermal resistance of the cooled electronic device will be investigated. A problem that is also worth considering in further investigations is the influence of the power consumed by the active components of forced cooling systems (Peltier modules, fans) on the running costs of the selected electronic devices.

Author Contributions: Conceptualization, K.G.; methodology, K.G., K.P.; validation, K.G., K.P.; investigation, K.P.; writing—original draft preparation, K.G., K.P.; writing—review and editing, K.G., K.P.; visualization, K.P.; supervision, K.G. All authors have read and agreed to the published version of the manuscript.

Funding: The project was financed within the framework of a program of the Ministry of Science and Higher Education called "Regionalna Inicjatywa Doskonałości" in the years 2019–2022, project number 006/RID/2018/19. The sum of the financing was 11,870,000 PLN.

Data Availability Statement: Data is contained within the article.

Conflicts of Interest: The authors declare no conflict of interest.

Abbreviations

a_i	coefficient corresponding to thermal time constant τ_{thi}
C_{thi}	thermal capacitance
d	thickness of the thermal pad
I_R	current of the investigated resistor
N	number of thermal time constants
p_P	power feeding the Peltier module
p_{th}	power dissipated in the investigated device
R_{th}	thermal resistance
R_T	resistance of the thermoresistor at temperature T_R
R_{T0}	resistance of the thermoresistor at temperature T_0
S	area of the thermal pad
t	time
T_0	reference temperature
T_R	temperature of the investigated resistor
v	airflow speed
V_R	voltage on the investigated resistor
$Z_{th}(t)$	transient thermal resistance
α	temperature coefficient of the resistance of the thermoresistor
λ	thermal conductivity
τ_{thi}	thermal time constant

References

1. Infineon, Transient Thermal Measurements and Thermal Equivalent Circuit Models, AN 2015-10, v. 1.2. 2020. Available online: https://www.infineon.com/dgdl/Infineon-Thermal_equivalent_circuit_models-ApplicationNotes-v01_02-EN.pdf?fileId=db3a30431a5c32f2011aa65358394dd2 (accessed on 29 January 2021).
2. Vassighi, A.; Sachdev, M. *Thermal and Power Management of Integrated Circuits*; Springer Science + Business Media: New York, NY, USA, 2006.
3. Perret, R. *Power Electronics Semiconductor Devices*; John Wiley & Sons: Hoboken, NJ, USA, 2009.
4. Di Napoli, F.; Magnani, A.; Coppola, M.; Guerriero, P.; D'Alessandro, V.; Codecasa, L.; Tricoli, P.; Daliento, S. On-Line Junction Temperature Monitoring of Switching Devices with Dynamic Compact Thermal Models Extracted with Model Order Reduction. *Energies* **2017**, *10*, 189. [CrossRef]
5. Lasance, C.J.M.; Poppe, A. (Eds.) *Thermal Management for LED Applications*; Springer: Dordrecht, The Netherlands, 2014.
6. Meyer, G. Heat Pipes & Vapor Chambers Design Gudelines, Webinar Thermal Live 2016. Available online: https://thermal.live/2016-event/technical-program/ (accessed on 29 January 2021).
7. Long, J.; Ogrenci-Memik, S.; Memik, G.; Mukherjee, R. Thermal monitoring mechanisms for chip multiprocessors. *ACM Trans. Arch. Code Optim.* **2008**, *5*, 1–33. [CrossRef]
8. De Falco, G.; Riccio, M.; Romano, G.; Maresca, L.; Irace, A.; Breglio, G. ELDO-COMSOL based 3D electro-thermal simulations of power semiconductor devices. In Proceedings of the IEEE Annual SEMIconductor THERMal Measurement, Modeling, and Management Symposium (SEMI-THERM), San Jose, CA, USA, 9–13 March 2014; pp. 35–40.
9. Riccio, M.; D'Alessandro, V.; Romano, G.; Maresca, L.; Breglio, G.; Irace, A. A Temperature-Dependent SPICE Model of SiC Power MOSFETs for Within and Out-of-SOA Simulations. *IEEE Trans. Power Electron.* **2018**, *33*, 8020–8029. [CrossRef]
10. Yener, Y.; Kakac, S. *Heat Conduction*; Taylor & Francis: Boca Raton, FL, USA, 2008.
11. Codecasa, L.; d'Alessandro, V.; Magnani, A.; Irace, A. Circuit-based electrothermal simulation of power devices by an ultrafast nonlinear MOS approach. *IEEE Trans. Power Electron.* **2016**, *31*, 5906–5916. [CrossRef]
12. Bahman, A.; Ma, K.; Blaabjerg, F. A Lumped Thermal Model Including Thermal Coupling and Thermal Boundary Conditions for High Power IGBT Modules. *IEEE Trans. Power Electron.* **2017**, *33*, 2518–2530. [CrossRef]
13. Castellazzi, A.; Kraus, R.; Seliger, N.; Schmitt-Landsiedel, D. Reliability analysis of power MOSFET's with the help of compact models and circuit simulation. *Microelectr. Reliab.* **2002**, *42*, 1605–1610. [CrossRef]
14. Narendran, N.; Gu, Y. Life of LED-based white light sources. *J. Disp. Technol.* **2005**, *1*, 167–171. [CrossRef]
15. Ciappa, M.; Carbognami, F.; Cora, P.; Fichtner, W. A novel thermomechanics-based lifetime prediction model for cycle fatigue failure mechnisms in power semiconductors. *Microelectron. Reliab.* **2002**, *42*, 1653–1658. [CrossRef]
16. Posobkiewicz, K.; Górecki, K. Wybrane komponenty układów chłodzenia przyrządów półprzewodnikowych. *Elektronika Konstr. Technol. Zastos.* **2020**, *61*, 11–18.
17. Biber, C. LED Light Emission as A Function of Thermal Conditions. In Proceedings of the 24th IEEE Semiconductor Thermal Measurement and Management Symposium, San Jose, CA, USA, 16–20 March 2008; pp. 180–184.
18. Heat Sink Manufacturer. Available online: https://celsiainc.com (accessed on 20 May 2020).

19. Custom Heat Pipes. Available online: https://myheatsinks.com/heat-pipe-solutions/custom-heat-pipes (accessed on 20 May 2020).
20. Ultra-Thin Heat Pipes. Available online: https://www.novarktechnologies.com/?p=30 (accessed on 20 May 2020).
21. Ultra Thin Vapor Chambers. Available online: https://www.boydcorp.com/thermal/two-phase-cooling/vapor-chambers/ultra-thin-vapor-chambers.html (accessed on 20 May 2020).
22. Vapor Chambers. Available online: https://www.cofan-usa.com/vapor-chambers (accessed on 20 May 2020).
23. News/Ultra Thin Vapor Chamber. 3 June 2019. Available online: https://trivision-etch.com/ultra-thin-vapor-chamber-2 (accessed on 20 May 2020).
24. ACT's Advancements in Vapor Chamber Technology. Available online: https://www.1-act.com/innovations/heat-pipes/vapor-chambers/?hilite=%27ceramic%27%2C%27vapor%27%2C%27chamber%27 (accessed on 20 May 2020).
25. Solution for Limited Space Application—Vapor Chamber. Available online: https://www.zaward.com/newsletter/45-Solution_for_limited_space_application.php (accessed on 20 May 2020).
26. Yang, H.W. Vapor Chamber Structure. U.S. Patent Application US 20190261537 A1, 22 August 2019.
27. You, S.M.; Kim, J.H.; Kwark, S.M.; Kim, J.J. Low-Profile Heat-Spreading Liquid Chamber Using Boiling. Patent Application WO 2008/118667 A2, 2 October 2008.
28. Thermally Conductive Materials. Available online: https://www.fischerelektronik.de/web_fischer/en_GB/heatsinks/E01/Thermal%20conductive%20material/index.xhtml (accessed on 20 May 2020).
29. Products. Available online: https://www.sheenthermal.com/product.html (accessed on 20 May 2020).
30. CPU Cooler. Available online: https://www.arctic.ac/eu_en/products/cooling/cpu.html (accessed on 20 May 2020).
31. Eriksen, A.S. Cooling System for a Computer System. U.S. Patent US10613601 B2, 7 April 2020.
32. Technology for Data Centers. Available online: https://www.asetek.com/data-center/technology-for-data-centers (accessed on 20 May 2020).
33. LIQTECH TR4 II 240. Available online: https://www.enermax.com/home.php?fn=eng/product_a1_1_1&lv0=109&lv1=124&no=395 (accessed on 20 May 2020).
34. CES 2020 Round-Up: MSI Launches the MAG CORELIQUID Range of AiO Coolers for CPus. Available online: https://www.msi.com/blog/CES2020-msi-liquid-cooler (accessed on 6 January 2020).
35. Thermoelectric Coolers Intro. Available online: https://www.tec-microsystems.com/faq/thermoelectic-coolers-intro.html (accessed on 20 May 2020).
36. TEC Ceramics. Available online: http://rmtltd.ru/technology (accessed on 20 May 2020).
37. Catalano, A.P.; Scognamillo, C.; d'Alessandro, V.; Castellazzi, A. Numerical Simulation and Analytical Modeling of the Thermal Behavior of Single- and Double-Sided Cooled Power Modules. *IEEE Trans. Compon. Packag. Manuf. Technol.* **2020**, *10*, 1446–1453. [CrossRef]
38. Chang, Y.; Li, W.H.; Luo, H.Z.; He, X.N.; Iannuzzo, F.; Blaabjerg, F.; Lin, W.X. A 3D Thermal Network Model for Monitoring Imbalanced Thermal Distribution of Press-Pack IGBT Modules in MMC-HVDC Applications. *Energies* **2019**, *12*, 1319. [CrossRef]
39. Górecki, K.; Zarębski, J.; Górecki, P.; Ptak, P. Compact thermal models of semiconductor devices—A review. *Int. J. Electron. Telecommun.* **2019**, *65*, 151–158.
40. Zajac, P.; Napieralski, A. Novel thermal model of microchannel cooling system designed for fast simulation of liquid-cooled ICs. *Microelectron. Reliab.* **2018**, *86*, 245–258. [CrossRef]
41. D'Alessandro, V.; Codecasa, L.; Catalano, A.P.; Scognamillo, C. Circuit-Based Electrothermal Simulation of Multicellular SiC Power MOSFETs Using FANTASTIC. *Energies* **2020**, *13*, 4563. [CrossRef]
42. D'Alessandro, V.; Catalano, A.P.; Codecasa, L.; Zampardi, P.J.; Moser, B. Accurate and efficient analysis of the upward heat flow in InGaP/GaAs HBTs through an automated FEM-based tool and Design of Experiments. *Int. J. Numer. Model. Electron. Netw. Devices Fields* **2019**, *32*, e2530. [CrossRef]
43. Catalano, A.P.; Scognamillo, C.; Castellazzi, A.; d'Alessandro, V. Optimum Thermal Design of High-Voltage Double-Sided Cooled Multi-Chip SiC Power Modules. In Proceedings of the 2019 25th International Workshop on Thermal Investigations of ICs and Systems (THERMINIC), Lecco, Italy, 25–27 September 2019; pp. 1–4. [CrossRef]
44. Poppe, A. Simulation of LED based luminaires by using multi-domain compact models of LEDs and compact thermal models of their thermal environment. *Microelectron. Reliab.* **2018**, *72*, 65–74. [CrossRef]
45. Scognamillo, C.; Catalano, A.P.; Lasserre, P.; Duchesne, C.; D'Alessandro, V.; Castellazzi, A. Combined experimental-FEM investigation of electrical ruggedness in double-sided cooled power modules. *Microelectron. Reliab.* **2020**, *114*, 113742. [CrossRef]
46. Górecki, K.; Górecki, P. Nonlinear Compact Thermal Model of the IGBT Dedicated to SPICE. *IEEE Trans. Power Electron.* **2020**, *35*, 13420–13428. [CrossRef]
47. Górecki, K.; Zarębski, J. The semiconductor device thermal model taking into account non-linearity and multipathing of the cooling system. *J. Phys. Conf. Ser.* **2018**, *494*, 012008. [CrossRef]
48. Górecki, K.; Zarębski, J. Nonlinear compact thermal model of power semiconductor devices. *IEEE Trans. Compon. Packag. Technol.* **2010**, *33*, 643–647. [CrossRef]
49. Datasheet of GBR-666 Thick Film Power Heater Series. Available online: https://www.tme.eu/Document/42f0713f39fe187f336fbd31efc6bdc4/gbr-666_en.pdf (accessed on 29 January 2021).

50. Technical Data of Proffuse Platinum Temperature Sensor PT1000-550. Available online: https://www.tme.eu/Document/67cf717905f835bc5efcdcd56ca3a8e2/Pt1000-550_EN.pdf (accessed on 29 January 2021).
51. Datasheet of Thermoelectric Module Ferrotec Nord TM–71-1.4-8.5MS. Available online: http://www.ferrotec-nord.com/wp-content/uploads/2018/08/TEM_Calc_install_v1.0_beta_build_0-1.zip (accessed on 29 January 2021).
52. Technical Card of Thermopads AG Thermopady. Available online: https://termopasty.pl/wp-content/uploads/2019/07/AG-thermopady-PL-1.pdf (accessed on 29 January 2021).
53. Specification Sheet of Freezer 34 eSports DUO. Available online: https://www.arctic.de/media/44/41/f0/1584088927/spec_sheet_Freezer_34_eSports_DUO_191106_r3_EN.pdf (accessed on 29 January 2021).
54. Székely, V. A new evaluation method of thermal transient measurement results. *Microelectron. J.* **1997**, *28*, 277–292. [CrossRef]
55. Bagnoli, P.E.; Casarosa, C.; Ciampi, M.; Dallago, E. Thermal Resistance Analysis by Induced Transient (TRAIT) Method for Power Electronic Devices Thermal Characterization—Part I: Fundamentals and Theory. *IEEE Trans. Power Electon.* **1998**, *13*, 1208–1219. [CrossRef]
56. Górecki, K.; Detka, K.; Górski, K. Compact Thermal Model of the Pulse Transformer Taking into Account Nonlinearity of Heat Transfer. *Energies* **2020**, *13*, 2766. [CrossRef]
57. Palankovski, V.; Quay, R. *Analysis and Simulation of Heterostructure Devices*; Springer: Wien, Austria, 2004.
58. Liebhard, J.H., IV; Liebhard, J.H., V. *A Heat Transfer Textbook*, 3rd ed.; Phlogiston Press: Cambridge, MA, USA, 2008.